AFRL-RZ-WP-TP-2010-2057

COLLISIONAL QUENCHING OF NO $A\,^2\Sigma^+(v' = 0)$ BETWEEN 125 AND 294 (POSTPRINT)

Campbell D. Carter

Propulsion Sciences Branch
Aerospace Propulsion Division

Thomas B. Settersten and Brian D. Patterson

Sandia National Laboratories

FEBRUARY 2010

AIR FORCE RESEARCH LABORATORY
PROPULSION DIRECTORATE
WRIGHT-PATTERSON AIR FORCE BASE, OH 45433-7251
AIR FORCE MATERIEL COMMAND
UNITED STATES AIR FORCE

REPORT DOCUMENTATION PAGE

Form Approved
OMB No. 0704-0188

1. REPORT DATE *(DD-MM-YY)*	2. REPORT TYPE	3. DATES COVERED *(From - To)*
February 2010	Journal Article Postprint	08 June 2007 – 08 April 2009

4. TITLE AND SUBTITLE
COLLISIONAL QUENCHING OF NO $A\,^2\Sigma^+(v' = 0)$ BETWEEN 125 AND 294 (POSTPRINT)

5a. CONTRACT NUMBER
In-house

5b. GRANT NUMBER

5c. PROGRAM ELEMENT NUMBER
61102F

6. AUTHOR(S)
Campbell D. Carter (AFRL/RZAS)
Thomas B. Settersten and Brian D. Patterson (Sandia National Laboratories)

5d. PROJECT NUMBER
2308

5e. TASK NUMBER
AI

5f. WORK UNIT NUMBER
2308AI00

7. PERFORMING ORGANIZATION NAME(S) AND ADDRESS(ES)
Propulsion Sciences Branch (AFRL/RZAS)
Aerospace Propulsion Division
Air Force Research Laboratory, Propulsion Directorate
Wright-Patterson Air Force Base, OH 45433-7251
Air Force Materiel Command, United States Air Force

Sandia National Laboratories
Combustion Research Facility
Livermore, CA 94551

8. PERFORMING ORGANIZATION REPORT NUMBER
AFRL-RZ-WP-TP-2010-2057

9. SPONSORING/MONITORING AGENCY NAME(S) AND ADDRESS(ES)
Air Force Research Laboratory
Propulsion Directorate
Wright-Patterson Air Force Base, OH 45433-7251
Air Force Materiel Command
United States Air Force

10. SPONSORING/MONITORING AGENCY ACRONYM(S)
AFRL/RZAS

11. SPONSORING/MONITORING AGENCY REPORT NUMBER(S)
AFRL-RZ-WP-TP-2010-2057

12. DISTRIBUTION/AVAILABILITY STATEMENT
Approved for public release; distribution unlimited.

13. SUPPLEMENTARY NOTES
Journal article published in *The Journal of Chemical Physics,* Vol. 130 (2009). Paper contains color. PA Case Number: 88ABW-2009-1233; Clearance Date: 26 Mar 2009.

14. ABSTRACT
We report measurements of the temperature-dependent cross sections for the quenching of fluorescence from the $A\,^2\Sigma^+(v' = 0)$ state of NO for temperatures between 125 and 294 K. Thermally averaged cross sections were measured for quenching by NO ($X\,^2\Pi$), N_2, O_2, and CO in a cryogenically cooled gas flow cell. Picosecond laser-induced fluorescence was time resolved, and the thermally averaged quenching cross sections were determined from the dependence of the fluorescence decay rate on the quencher-gas pressure. These measurements extend to lower temperature the range of previously published results for NO and O_2 and constitute the first reported measurements of the N_2 and CO cross sections for temperatures below 294 K. Between 125 and 294 K, a negative temperature dependence is observed for quenching by NO, O_2, and CO, implicating collision-complex formation in all three cases. Over the same temperature range, a constant, nonzero cross section is measured for quenching by N_2. Updated empirical models for the temperature dependence of the cross sections between 125 and 4500 K are recommended.

15. SUBJECT TERMS

16. SECURITY CLASSIFICATION OF:			17. LIMITATION OF ABSTRACT:	18. NUMBER OF PAGES	19a. NAME OF RESPONSIBLE PERSON (Monitor)
a. REPORT	b. ABSTRACT	c. THIS PAGE			Campbell D. Carter
Unclassified	Unclassified	Unclassified	SAR	16	19b. TELEPHONE NUMBER *(Include Area Code)* N/A

Standard Form 298 (Rev. 8-98)
Prescribed by ANSI Std. Z39-18

Collisional quenching of NO $A\ ^2\Sigma^+(v'=0)$ between 125 and 294 K

Thomas B. Settersten,[1,a)] Brian D. Patterson,[1] and Campbell D. Carter[2]
[1]*Combustion Research Facility, Sandia National Laboratories, Livermore, California 94551, USA*
[2]*Air Force Research Laboratory, AFRL/RZA Wright-Patterson Air Force Base, Ohio 45433, USA*

(Received 14 April 2009; accepted 28 April 2009; published online 22 May 2009)

We report measurements of the temperature-dependent cross sections for the quenching of fluorescence from the $A\ ^2\Sigma^+(v'=0)$ state of NO for temperatures between 125 and 294 K. Thermally averaged cross sections were measured for quenching by NO($X\ ^2\Pi$), N_2, O_2, and CO in a cryogenically cooled gas flow cell. Picosecond laser-induced fluorescence was time resolved, and the thermally averaged quenching cross sections were determined from the dependence of the fluorescence decay rate on the quencher-gas pressure. These measurements extend to lower temperature the range of previously published results for NO and O_2 and constitute the first reported measurements of the N_2 and CO cross sections for temperatures below 294 K. Between 125 and 294 K, a negative temperature dependence is observed for quenching by NO, O_2, and CO, implicating collision-complex formation in all three cases. Over the same temperature range, a constant, nonzero cross section is measured for quenching by N_2. Updated empirical models for the temperature dependence of the cross sections between 125 and 4500 K are recommended based on weighted least-squares fits to the current low-temperature results and previously published measurements at higher temperature. The results of over 250 measurements presented here indicate that the collisionless lifetime of NO $A\ ^2\Sigma^+(v'=0)$ is approximately 192 ns. © *2009 American Institute of Physics*. [DOI: 10.1063/1.3138178]

I. INTRODUCTION

Nitric oxide (NO) is a prevalent combustion by-product, and laser-induced fluorescence (LIF) in the NO gamma bands is often used as a diagnostic in combustion research.[1] Because NO is relatively stable, it is also often used as a seed species for thermometry and/or mixing studies.[2] Furthermore, NO can easily be added to air without changing significantly the net molecular weight, and thus it is ideal as a seed species in studies involving compressible flows.[3] Herein, expansion of the gas to supersonic flow velocity results in a reduced temperature: with an initial air temperature of 295 K, expansion to Mach 2 flow speed results in an air temperature of 164 K, a value for which heretofore there were no available quenching data.

Converting the LIF signal into a quantitative concentration measurement requires correction for variation in the fluorescence quantum yield, which depends on the rate of electronic quenching collisions. In a previous publication, we applied time-resolved LIF using a picosecond-duration laser and a microchannel-plate photomultiplier tube (MCP-PMT) detector to characterize with unprecedented precision the temperature- and species-dependent quenching of NO $A\ ^2\Sigma^+(v'=0)$ between 294 and 1300 K.[4] These results were used in combination with measurements at higher temperatures to generate empirical models of the thermally averaged quenching cross sections. These models predicted fluorescence decay rates that agreed to within 5% of the rates measured in an atmospheric-pressure diffusion flame,[5] where previously accepted quenching models[6,7] underpredicted the measured rates by as much as 32%.

Although the models recommended in Ref. 4 improve the accuracy of prediction of quenching rates for temperatures at or above 294 K, extrapolation of these models to temperatures below room temperature was not recommended. Prediction of the quenching rate at low temperatures is particularly important for NO LIF measurements in the upper atmosphere and in low-temperature supersonic flows. With the exception of N_2, the cross sections of all investigated species in Ref. 4 increased with decreasing temperature around 300 K, leading to a significant increase in the predicted cross section when extrapolated to temperatures less than 294 K. This result underscores the importance of an attractive intermolecular potential for molecular complexes involving NO $A\ ^2\Sigma^+$ (Ref. 8) and motivates the current investigation.

Zhang and Crosley[8] performed the only previous systematic investigation of low-temperature quenching of NO $A\ ^2\Sigma^+$. In that work, the authors used time-resolved LIF excited by a nanosecond-duration laser to infer cross sections for quenching by CO_2, O_2, H_2O, NH_3, H_2S, and NO($X\ ^2\Pi$) between 215 and 300 K. In the current work, we extend the lower end of the temperature range to 125 K and use picosecond time-resolved LIF to investigate quenching by O_2, N_2, NO($X\ ^2\Pi$), and CO.

II. EXPERIMENTAL DETAILS

Time-resolved fluorescence signals were recorded for specific gas mixtures in a temperature- and pressure-

a)Electronic mail: tbsette@sandia.gov.

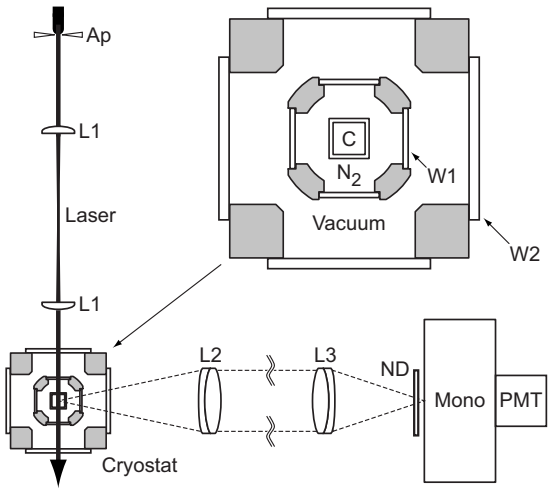

FIG. 1. Experimental arrangement with section detail of cryostat shown on top right of the figure. Ap: 1.5 mm aperture; L1: 250 mm focal-length fused silica singlet lens; L2: 150 mm focal-length UV achromatic doublet lens; L3: 100 mm focal-length achromatic doublet lens; ND: neutral density filters; Mono: 1/8 m monochromator; PMT: MCP-PMT; C: ES quartz fluorimeter cell with UV BBAR coating; W1 and W2: S1-UV windows with UV BBAR coating (four each).

controlled flow cell. Thermally averaged quenching cross sections were determined from the pressure dependence of the fluorescence decay rate. The experimental setup consisted of a picosecond dye laser, a fluorescence detection/recording system, a cooled flow cell, and a gas-mixing manifold.

The picosecond dye laser was a pulse-amplified distributed-feedback dye laser (DFDL) similar to that described in Refs. 4 and 9. The second-harmonic output of a regeneratively amplified neodymium doped yttrium aluminum garnet laser, which was seeded by a bandwidth-limited mode-locked laser producing pulses of approximately 100 ps duration, was used to pump a DFDL, a side-pumped dye amplifier, and an end-pumped dye amplifier. The amplified output was frequency tripled in two β-barium borate crystals to produce ultraviolet (UV) pulses with an estimated pulse width of 50 ps. The laser was tuned to 226.87 nm to excite the $P_2+{}^QP_{12}$ band head of the NO $A\ ^2\Sigma^+(v'=0)-X\ ^2\Pi(v''=0)$ system. Based on an approximate laser line width of 1 cm^{-1}, we estimate that the laser excited NO molecules to rotational levels in $A\ ^2\Sigma^+(v'=0)$ with $1\leq N'\leq 4$. A 1.5-mm-diameter aperture selected the central uniform part of the UV beam, which was relay imaged into the center of the fluorescence flow cell using two 250-mm focal-length lenses, as depicted in Fig. 1. We limited the laser-pulse energy to approximately 5 μJ to avoid significant ionization and subsequent photochemistry in the sample volume. We verified by measurement and simulation[10] that the corresponding laser intensity produced linear excitation of the NO for all experimental conditions.

The detection channel monitored fluorescence in the $A-X(0,2)$ band. Fluorescence was collected from the center of the flow cell, normal to the laser propagation direction, using a 150-mm focal-length, 50-mm-diameter UV achromatic doublet lens. A second achromatic doublet lens with a 100 mm focal length imaged the collected fluorescence onto the slit of a 1/8-m monochromator. The two lenses were separated by approximately 30 cm to limit collection primarily to the center of the cell, suppressing background caused by elastic scattering from the cell windows. The monochromator produced a measured trapezoidal bandpass centered at 245 nm with a full width at half maximum of 10.5 nm and uniform transmission over the central 7 nm. The large bandpass ensured detection of fluorescence from all rotational levels in $A\ ^2\Sigma^+(v'=0)$, including those populated by rotational energy transfer. A MCP-PMT was used to detect the fluorescence signal, which was digitized and averaged using a digital storage oscilloscope with a 1-GHz analog bandwidth. The MCP-PMT was biased with -3 kV for all measurements, and the signal level was kept well within the linear range of the detector by using neutral density filters to attenuate the fluorescence when necessary.

The fluorescence flow cell was constructed from a $1.0\times1.0\times3.3$ cm^3 flow-through cell with ES-grade quartz windows (NSG Precision Cells, Inc., type-501FL). A broadband (200–300 nm) antireflection coating (BBAR) was applied to the outside surfaces of the cell. Temperature control of the fluorescence cell was achieved by adapting a liquid-nitrogen-cooled, variable-temperature cryostat (Janis Research Co., model VNF-100) so that the fluorescence cell could be placed in the flowing, temperature-controlled N_2 vapor. The sample positioner of the cryostat was modified to accommodate the fluorescence cell and gas supply tubing, and a UV BBAR coating was applied to both sides of all cryostat windows (see Fig. 1). The test gas flowed to and from the cell through approximately 70 cm of thin-walled, 1-mm inner-diameter, stainless-steel capillary tubing, which passed through O-ring seals at the top of the sample column. Liquid nitrogen was boiled through a temperature-controlled nozzle in the bottom of the sample column and flowed upward past the fluorescence cell. Matched silicon diode temperature sensors that were located on the heated nozzle and above the top of the cell continuously monitored the temperature. During operation, the nozzle temperature was typically regulated to within 0.1 K of experimental set points ranging from 125 to 294 K, and the gradient between the two sensors was typically less than 1 K. In separate experiments, a 250-μm-diameter thermocouple probe was inserted through the gas supply capillary to the cell and verified that the test gas temperature was equal to that of the flowing N_2 vapor for all flow conditions.

The cell was evacuated to less than 10^{-5} Torr using an oil-free pumping system consisting of a turbomolecular pump backed by a dry scroll pump. The measured leak rate of the cell was less than 10^{-4} SCCM (SCCM denotes cubic centimeter per minute at STP). For all experiments, a single mass-flow controller sets the flow rate of the test gas. A precision metering valve on the outlet was used to manually adjust the cell pressure in the 50–300 Torr range. The gas pressures at the input and outlet of the cryostat were monitored using high-precision, 1000-Torr capacitance manometers, and the pressures were logged during all experiments. The capacitance manometers were zeroed at $<10^{-4}$ Torr and calibrated at atmospheric pressure with a Fortin-type mercurial barometer. For static conditions, the calibrated pressure

readings agreed to better than 0.2% over the course of all experiments. The pressure drops between the cell and the locations of the input and outlet manometers were calibrated at all experimental pressure conditions by replacing the cell with a third capacitance manometer.

Most experiments were conducted with a flow rate of 10 SCCM because of the increased uncertainty in the calculated cell pressure caused by the large pressure drops in the capillary tubing that were produced by higher flow rates. For the range of temperatures and pressures investigated, the time to exchange the gas within the sample volume for 10 SCCM flow ranged from 50 to 800 ms, which corresponds to 1–16 laser shots. To check for dependence of the results on the flow rate, higher flow rates of up to 100 SCCM were used to ensure complete exchange during the intralaser-pulse period. For the majority of the gas mixtures, for which the quenching rate coefficients were on the order of 10^5 s^{-1} $Torr^{-1}$ or greater, the measured quenching rate coefficients using flow rates between 10 and 100 SCCM were within the scatter of repeated measurements. Only in mixtures of trace ($\leq$1000 ppm) NO in N_2, for which the quenching rate coefficients were on the order of 10^4 s^{-1} $Torr^{-1}$ or less, was a discernible effect observed. In this case, the measured quenching rate coefficients using a 10 SCCM flow rate typically exceeded those using a 50 SCCM or greater flow rate by approximately $(1-2)\times10^3$ s^{-1} $Torr^{-1}$. For these very weakly quenching mixtures, only data obtained with a flow rate of 100 SCCM were used in the analysis.

Gas mixtures were prepared in a high-purity mixing manifold using ultrahigh-purity (UHP) N_2, UHP O_2, UHP CO, and either chemically pure (CP) grade NO (99%) or a certified mixture of 99 ppm NO in UHP nitrogen. Nitrogen was further purified with an oxygen scrubber. The manifold consisted of three 4-L high-purity sample bottles that could be used individually or in parallel. Prior to the preparation of each mixture, the manifold was evacuated to less than 10^{-6} Torr using a dedicated oil-free pumping system. Partial pressures of the gases were measured using calibrated 10- and 1000-Torr capacitance manometers. The total mixture pressures were approximately 1000 Torr.

Typically, fluorescence decays for each gas mixture were collected in a sequence of five or six pressures for each temperature. The oscilloscope sampling rate and trigger point were set so that each 1000-point record included a preexcitation baseline and at least eight e-folding times of the LIF decay to ensure full recovery to the signal baseline. The oscilloscope averaged the fluorescence decays from 256 laser pulses, and the averaged waveforms were downloaded to a computer. Typically, three to five such waveforms were sequentially acquired and subsequently averaged in software to produce low-noise records for accurate fitting. No background subtraction was necessary, and peak signal-to-noise ratios of greater than 10^3 were achieved. This acquisition sequence was typically repeated five to ten times at each pressure setting to establish measurement reproducibility.

Prior to each pressure sequence, at least ten acquisitions were analyzed to ensure good reproducibility of the measured fluorescence decay rate at a fixed flow condition. When the measurement reproducibility was poor and a clear trend (either increasing or decreasing decay rate) with time was observed, the system was purged several times and the gas mixture flowed until good measurement reproducibility (typically less than 3% variation) was demonstrated.

III. ANALYSIS

A convolve-and-compare fitting routine[4,9] was used to determine the fluorescence decay rate γ_{mix} from the averaged fluorescence decay records. The fitting routine accounted for the impulse-response function (IRF) of the detection electronics. The IRF, which was measured using elastic scattering of the picosecond laser, characterizes the collective response of the detector, the oscilloscope, and the cabling between the detector and the oscilloscope.

The fluorescence decay rate γ_{mix} for a particular gas mixture at temperature T and pressure P depends on the quenching rate coefficient q_{mix} of the mixture:

$$\gamma_{\text{mix}}(T,P) = \frac{1}{\tau_{\text{rad}}} + Pq_{\text{mix}}(T), \tag{1}$$

where τ_{rad} is the radiative lifetime of the excited state. We determined q_{mix} by fitting Eq. (1) to the experimentally measured fluorescence decay rates as a function of the mixture pressure. Although we have previously measured the inverse of the natural radiative lifetime $1/\tau_{\text{rad}}=5.2\times10^6$ s^{-1} for NO $A\ ^2\Sigma^+(v'=0)$,[4,11] we allowed it to vary as a fitting parameter in the current experiments and use the results from the analysis to update the recommended value of the lifetime.

The quenching rate coefficient for a particular mixture depends on its chemical composition and on the quenching rate coefficients q_j for each of the constituent species j:

$$q_{\text{mix}}(T) = \sum_j X_j q_j(T), \tag{2}$$

where X_j is the mole fraction of species j. The simplest mixtures in the current experiment consisted of NO and N_2. In this case, the rate coefficient for the mixture can be written in terms of the NO mole fraction,

$$q_{\text{NO/N}_2}(X_{\text{NO}},T) = q_{\text{N}_2}(T) + X_{\text{NO}}[q_{\text{NO}}(T) - q_{\text{N}_2}(T)]. \tag{3}$$

The quenching rate coefficients for NO and N_2 were determined by fitting Eq. (3) to the measured rate coefficients for a series of NO concentrations.

To determine quenching rate coefficients for O_2 and CO, either gas was mixed in varying concentrations with a premixed dilute mixture of approximately 100 ppm NO in N_2. In this case, the quenching rate coefficient for the three-species mixture is written as

$$q_{j/\text{NO/N}_2}(X_j,T) = q_{\text{NO/N}_2}(T) + X_j[q_j(T) - q_{\text{NO/N}_2}(T)], \tag{4}$$

where j represents either O_2 or CO. The quenching rate coefficient q_j was determined by fitting Eq. (4) to the measured mixture rate coefficients for a series of O_2 or CO concentrations.

The effect of impurities in the gas streams was analyzed based on the manufacturer's guaranteed specification of trace constituents in the bottled gases. The measurement of q_{N_2} is the most sensitive to trace levels of impurities because N_2 is

an extremely inefficient quenching partner. To minimize the effect of impurities, we used bottled UHP-grade N_2 and further reduced the level of the O_2 impurity to less than 0.015 ppm with an oxygen scrubber. As a result, we estimate that the effect of impurities on the measurement of q_{N_2} is less than 1%. Because the other three gases investigated here are all effective quenchers, the measurements of their quenching rate coefficients are less susceptible to compromise by impurities. The effect of impurities in the CP-grade NO on the measurement of q_{NO} is less than 0.2%, and the effects of impurities in the UHP-grade O_2 and CO on the measurements of q_{O_2} and q_{CO} are even less significant.

The fitted quenching rate coefficients for NO($X\ ^2\Pi$), N_2, O_2, and CO were converted to thermally averaged quenching cross sections σ using[12]

$$\sigma_j(T) = q_j(T)\sqrt{\frac{\pi\mu_j k_B T}{8}}, \tag{5}$$

where μ_j is the reduced mass of the NO/quencher collision pair, and k_B is Boltzmann's constant.

The current measurements correspond to quenching from relatively low N' thermal distributions in $A\ ^2\Sigma^+(v'=0)$. Laser excitation in the $P_2+{}^QP_{12}$ band head populated $N'=1-4$ of $(v'=0)$. The rotational distribution of the laser-excited population rapidly thermalized early in the fluorescence decays because the high N_2 dilution (>92%) used in these experiments produced rotational energy transfer rates[13–15] that were between 20 and 10^4 times larger than the electronic quenching rates of the gas mixtures. The thermal distribution peaks between $N'=4$ and 7 for the range of temperatures investigated. The current analysis did not explicitly account for rotational levels in the fluorescing excited state because prior investigators[16–18] have not observed a measurable rotational-level dependence for quenching in $A\ ^2\Sigma^+(v'=0)$ for a variety of collision partners, including those studied here. The high quality of the model fits to all of the fluorescence decay data further supports the use of this simplification in the analysis. Thus, we expect that comparisons are valid between the current and previous measurements of thermally averaged quenching cross sections using excitation to different rotational levels in $(v'=0)$.

IV. RESULTS

We analyzed over 10 000 averaged fluorescence decays for approximately 90 gas mixtures and eight temperatures. Panels (a) and (b) of Fig. 2 present examples of dc-baseline-corrected data and the corresponding fits for fluorescence signals with decay rates of $\gamma_{mix}=5.60\times10^6$ and 177×10^6 s^{-1}, respectively. These decay rates approximately span the range of rates measured in the current experiments. Note that the weak cable reflection at approximately 10 ns caused a significant shift in the signal in Fig. 2(b), and the convolve-and-compare approach was essential for satisfactory fitting of the signal and accurate measurement of γ_{mix}. Repeated decay-rate measurements for a particular gas mixture, temperature, and pressure typically agreed to within 3%.

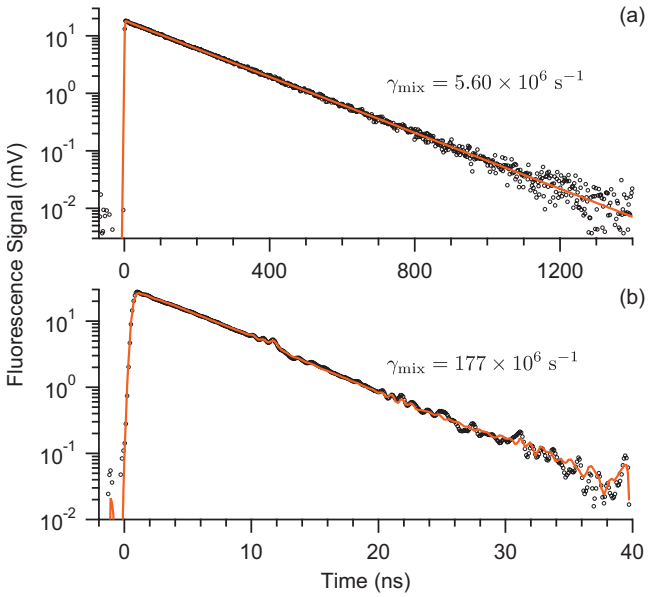

FIG. 2. (Color) Examples of convolve-and-compare fitting (solid curves) to two dc-baseline-corrected fluorescence decays (circles) for mixtures of (a) 99 ppm NO in N_2 at 125 K and 101 Torr and (b) 5% O_2 and 94 ppm NO in N_2 at 125 K and 297 Torr. Best-fit values of γ_{mix} are shown.

The γ_{mix} versus P data from over 250 pressure sequences were fitted with Eq. (1), and excellent linearity was observed in all cases. Figure 3 shows an example of the determination of the quenching rate coefficient for a mixture of 1% O_2 and 98 ppm NO in N_2 at 175 K. The data shown for two pressure sequences, each consisting of 37 decay-rate measurements at five pressures, demonstrate excellent reproducibility; the fitted rate coefficients agree to within the 2-σ fitting uncertainty of approximately 1%. In addition to recording the best-fit values of q_{mix} for each pressure sequence, we recorded the best-fit values of the zero-pressure intercepts to determine the natural lifetime of NO $A\ ^2\Sigma^+(v'=0)$, τ_{rad}. The weighted means of the results for each temperature setting are listed in Table I.

Equations (3) and (4) were used to fit the q_{mix} versus X_j data to determine the species-specific quenching rate coeffi-

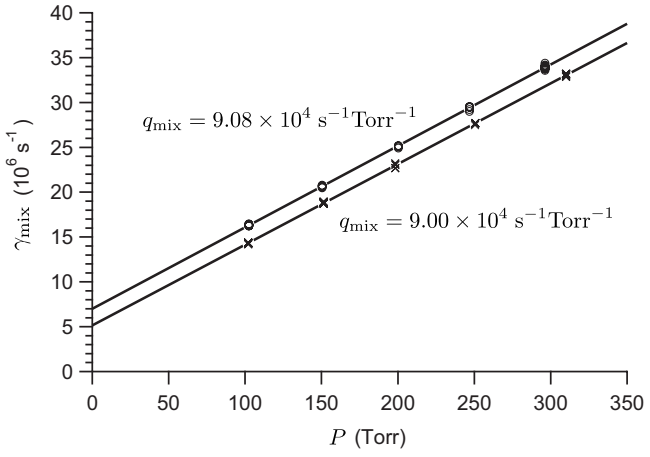

FIG. 3. Examples of LIF–decay-rate data and corresponding model fits using Eq. (1) for two pressure sequences of a mixture of 1% O_2 and 98 ppm NO in N_2 at 175 K. The top sequence has been offset by 2×10^6 s^{-1} for clarity.

TABLE I. Summary of best-fit values of NO $A\ ^2\Sigma^+(v'=0)$ lifetime obtained from zero-pressure intercepts of γ_{mix} vs P data. Values listed in parentheses represent the 2-σ statistical uncertainty.

T (K)	Number of fits	τ_{rad} (ns)
125	17	192.6 (0.5)
150	27	192.6 (0.3)
175	25	190.4 (0.4)
200	41	192.1 (0.2)
225	20	189.0 (0.4)
250	20	190.3 (0.5)
275	12	191.4 (0.7)
294	93	192.0 (0.1)

cients. Figure 4 shows the data for NO/N_2 mixtures at 294 K fitted with Eq. (3). In this case, the slope at large NO concentration is primarily determined by the quenching rate coefficient for NO, and the $X_{NO}=0$ intercept is the quenching rate coefficient for N_2. The data for NO/N_2 mixtures at seven other temperatures, $O_2/NO/N_2$ mixtures at eight temperatures, and $CO/NO/N_2$ mixtures at two temperatures were similarly analyzed. Table II includes the complete listing of the best-fit values for the temperature-dependent quenching rate coefficients and the corresponding thermally averaged cross sections for NO, N_2, O_2, and CO that were determined in the current experiments.

As in Ref. 4, we use simplified empirical functions to parametrize the temperature dependence of the measured cross sections:

$$\sigma(T) = c_0 + c_1 e^{+c_2/T} + c_3 e^{-c_4/T}, \tag{6}$$

$$\sigma(T) = c_0 + c_1 (300/T)^{c_2} + c_3 e^{-c_4/T}. \tag{7}$$

Best-fit values for the parameters were determined using weighted least-squares fits to measured cross sections. The c_0 term accounts for the small nonzero cross section that is measured for quenching by N_2, but, in accord with our previous analyses,[4] c_0 is forced to zero when fitting the cross-section data for quenching by the other molecules. The current low-temperature data for NO, O_2, and CO are most

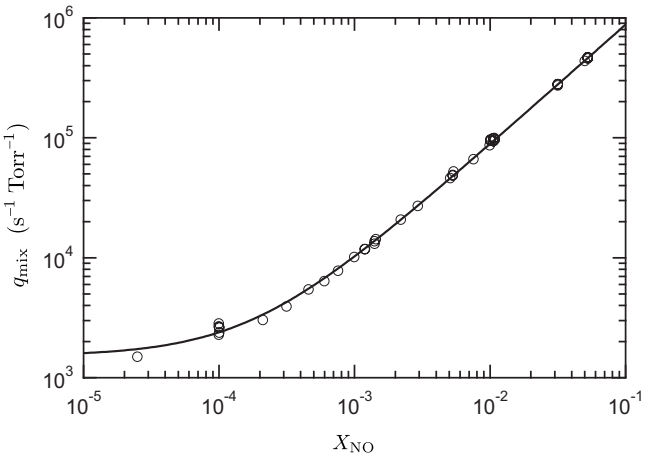

FIG. 4. Measured quenching rate coefficients for NO/N_2 mixtures at 294 K (circles). Equation (3) was fitted to the data (solid curve) to yield best-fit values of $q_{NO}=8.77\times10^6$ s^{-1} $Torr^{-1}$ and $q_{N_2}=1.5\times10^3$ s^{-1} $Torr^{-1}$.

TABLE II. Summary of measurements. Values listed in parentheses represent 2-σ fitting uncertainty.

Quencher	T (K)	q (10^6 s^{-1} $Torr^{-1}$)	σ (Å^2)
NO($X\ ^2\Pi$)	125	15.93 (0.30)	49.1 (0.9)
	150	14.04 (0.12)	47.4 (0.4)
	175	12.20 (0.13)	44.5 (0.5)
	200	11.96 (0.09)	46.6 (0.3)
	225	10.97 (0.09)	45.3 (0.4)
	250	9.90 (0.20)	43.1 (0.9)
	275	9.21 (0.13)	42.1 (0.6)
	294	8.77 (0.20)	41.4 (0.9)
N_2	125	2.98 (0.64)$\times10^{-3}$	9.02 (1.95)$\times10^{-3}$
	150	2.59 (0.30)$\times10^{-3}$	8.60 (0.98)$\times10^{-3}$
	175	2.47 (0.30)$\times10^{-3}$	8.83 (1.08)$\times10^{-3}$
	200	2.00 (0.25)$\times10^{-3}$	7.67 (0.97)$\times10^{-3}$
	225	1.63 (0.25)$\times10^{-3}$	6.60 (1.03)$\times10^{-3}$
	250	2.38 (0.58)$\times10^{-3}$	10.20 (2.47)$\times10^{-3}$
	275	2.48 (0.58)$\times10^{-3}$	11.15 (2.59)$\times10^{-3}$
	294	1.52 (0.30)$\times10^{-3}$	7.04 (1.39)$\times10^{-3}$
O_2	125	11.37 (0.10)	35.6 (0.3)
	150	9.70 (0.05)	33.3 (0.2)
	175	8.62 (0.07)	31.9 (0.2)
	200	7.81 (0.04)	30.9 (0.2)
	225	7.17 (0.05)	30.1 (0.2)
	250	6.63 (0.04)	29.4 (0.2)
	275	6.15 (0.05)	28.5 (0.2)
	294	5.94 (0.02)	28.5 (0.1)
CO	125	4.50 (0.06)	13.6 (0.2)
	175	2.80 (0.02)	10.0 (0.1)

sensitive to the parameters c_1 and c_2 in the second term on the right-hand sides of Eqs. (6) and (7). The third term on the right-hand sides of both equations, which is defined by parameters c_3 and c_4, is included to account for the increase in the cross section at high temperature that occurs for all four species considered here.[4]

The second term on the right-hand side of Eq. (6) simulates the low-temperature behavior associated with an attractive intermolecular potential where the fitting parameter c_2 represents the well depth. This exponential form for the cross section is described by Lin *et al.*[19] and has been used previously to describe the negative temperature dependence of cross sections for quenching of NO $A\ ^2\Sigma^+$ by H_2O,[8,18] CO_2,[4,8,18] O_2,[4,8] NO $X\ ^2\Pi$,[4,8] and CO.[4]

In Eq. (7), the negative temperature dependence of the cross section is modeled using a power-law expression instead of an exponential term. This approach follows Holtermann *et al.*,[20] who derived classical expressions of the capture cross section for formation of a collision complex based on a multipole expansion of the intermolecular potential. The temperature exponent c_2 in Eq. (7) depends on the particular form of the potential. A temperature exponent of 1/3 is predicted for complex formation via dispersion or dipole-induced dipole interactions, and a temperature exponent of 2/3 is predicted for complex formation via dipole-dipole interaction.[20] The relative importance of these interactions

TABLE III. Empirical models for temperature-dependent cross sections.

	Equation (6): $\sigma=c_0+c_1e^{c_2/T}+c_3e^{-c_4/T}$					Equation (7): $\sigma=c_0+c_1(300/T)^{c_2}+c_3e^{-c_4/T}$				
Quencher	c_0 (Å^2)	c_1 (Å^2)	c_2 (K)	c_3 (Å^2)	$c_4/1000$ (K)	c_0 (Å^2)	c_1 (Å^2)	c_2	c_3 (Å^2)	$c_4/1000$ (K)
NO	{0}[a]	34.8(0.4)[b]	48.5(2.9)	13.3(2.4)	2.69(0.65)	{0}	40.8(0.2)	0.22(0.02)	25.8(1.3)	1.39(0.14)
N_2	0.008(0.001)	2.04(0.15)	−2250(74)	96(46)	12.7(1.9)					
O_2	{0}	22.5(0.2)	61.9(1.8)	{7.41}	{3.80}	{0}	27.5(0.3)	0.29(0.02)	15.7(2.1)	1.29(0.29)
CO	{0}	3.82(0.08)	163(5)	15.8 (1.5)	1.74(0.11)	{0}	6.26(0.12)	0.86(0.04)	14.8(0.8)	1.08(0.07)

[a]All values in { } were held constant in the fits.
[b]All values in ( ) represent 2-σ fitting uncertainty.

can be approximated from the permanent dipole moments, polarizabilities, and ionization potentials of the collision partners.[20,21]

Table III lists the empirical models and weighted fits to the temperature-dependent data for NO, N_2, O_2, and CO. Cross-section measurements from the current experiments and from Ref. 4 were used for $T<1300$ K because of their much higher precision relative to earlier measurements in this temperature range. For $T>1300$ K, measurements from shock-tube studies were used.[22–24]

V. DISCUSSION

A. NO $A\ ^2\Sigma^+(v'=0)$ lifetime

In previous work,[4] we reported measurements of the collisionless lifetime of NO $A\ ^2\Sigma^+(v'=0)$ that ranged from 187 to 197 ns. The result obtained from the ten zero-pressure intercepts at 294 K was 194.0 ± 0.5 ns, which is approximately 6% smaller than the most recent recommendation of 205 ± 7 ns by Luque and Crosley.[25,26] In consideration of those and previously published results, we suggested in Ref. 4 that our measurement should be viewed with some caution. Since that publication, however, a separate experiment conducted by our group yielded a natural lifetime of 193 ns using time-resolved LIF measurements,[11] and the mean value of the natural lifetime inferred from the 255 current measurements shown in Table I is 191.8 ± 0.1 ns. Based on the consistency of our results in three separate experiments and the superior precision of our approach and its insensitivity to the electronic artifacts that can compromise the accuracy of lifetime measurements,[4] we recommend the value of 192 ns ($\tau_{rad}^{-1}=5.21\times10^6$ s^{-1}). Updated measurements of the natural lifetimes of NO $A\ ^2\Sigma^+(v'=0,1,2)$ will be presented in a subsequent publication.

B. Quenching by NO

Figure 5(a) displays the current measurements of the thermally averaged self-quenching cross section for $125\leq T<300$ K. Note that error bars representing the statistical fitting uncertainty are obscured by the symbols for the current data. The results agree well with the only other reported low-temperature measurements,[8] which are also shown in Fig. 5(a).

Although the current work focuses on quenching behavior at low temperature, we parametrize the results in terms of Eq. (6) or Eq. (7) for temperatures that range from 125 to 4500 K. Figure 5(b) displays the data on an expanded abscissa that spans this temperature range and also includes previous results for $T\geq294$ K. In this case, only the data that were considered in the fitting analysis were plotted. Below 1300 K, the analysis included the current results and those from Ref. 4 because of their much higher precision relative to earlier temperature-dependent measurements.[8,18,27] Above 1300 K, results from shock-tube studies[22–24] were used. Fits to the data using Eqs. (6) and (7) are shown, respectively, as the thick solid curves and the thick dotted-dashed curves in Fig. 5. Table IV lists authors, plot symbols, and references for this figure and all similar plots of σ versus T shown subsequently.

Based on a harpoon quenching mechanism, Paul *et al.*[6] recommended a constant self-quenching cross section of 43 Å^2 (dashed lines in Fig. 5). Zhang and Crosley[8] were the first to observe evidence of collision-complex formation in NO self-quenching in their measurements between 215 and 294 K. Based on an evaluation of their low-temperature data and previously published measurements at elevated temperature, they modeled the temperature dependence of the quenching cross section using the two-parameter Parmenter formalism ($\sigma=\sigma_\infty e^{+\epsilon/k_BT}$).[19] The reported well depth of

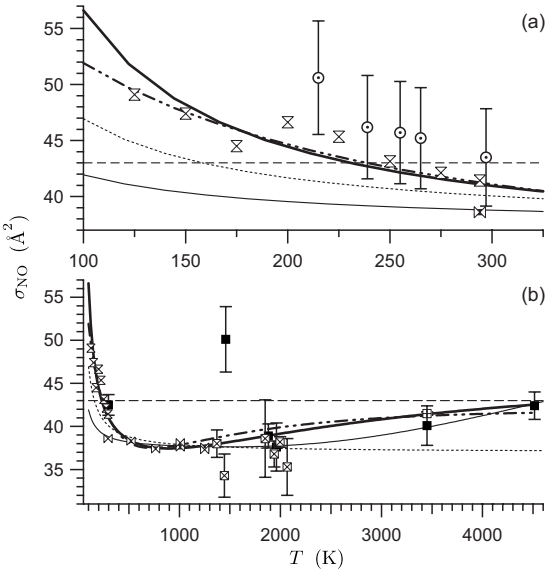

FIG. 5. Temperature dependence of the self-quenching cross section. (a) Comparison of current and previous low-temperature measurements and models. (b) Measurements used in global fit for $125\leq T\leq4500$ K. See Table IV for the legend to symbols and line types.

TABLE IV. Legend for Figs. 5–8.

Measured Cross Sections	Symbol	Ref.
Settersten *et al.*	⧖	Present Work
Settersten *et al.*	⋈	[4]
Gray, Paul, and Durant	⊠	[22]
Thoman *et al.*	⊞	[23]
Zhang and Crosley	⊙	[8]
Paul *et al.*	■	[24]

Models	Line Style	Ref.
Settersten *et al.* (Eq. 6)	———	Present Work
Settersten *et al.* (Eq. 7)	—·—·—	Present Work
Settersten *et al.*	———	[4]
Paul *et al.*	– – – – –	[6]
Tamura *et al.*	·····	[7]

$\epsilon=33\ \text{cm}^{-1}$ and high-temperature asymptote of $\sigma_\infty=37\ \text{Å}^2$ produced the dotted curves shown in Fig. 5. We observed evidence of complex formation for $T>294$ K in our previous measurements,[4] which showed a slight decrease in the self-quenching cross section for increasing temperature between 294 and 765 K. However, the fit to the data recommended in Ref. 4, shown as the thin solid curves in Fig. 5, corresponds to a much shallower well depth ($8\ \text{cm}^{-1}$) that clearly underestimates the temperature dependence of the self-quenching cross section when extrapolated to temperatures below 294 K.

When the current data are included in the analysis, the best-fit value of the c_2 parameter in Eq. (6) corresponds to a well depth of $34\ \text{cm}^{-1}$, in excellent agreement with the well depth reported by Zhang and Crosley.[8] The current least-squares fit using Eq. (6) [thick dotted-dashed curve in Fig. 5(a)] agrees significantly better with both sets of low-temperature measurements than the previously recommended models.[4,8] As is evident in Fig. 5(a), a slightly better fit to the lowest-temperature data results when the power-law expression [Eq. (7)] is used. In this case, the c_2 parameter is the temperature exponent, and the best-fit value of 0.22 is more consistent with that predicted for complex formation through an electrostatic interaction that is dominated by dispersion or dipole-induced dipole forces rather than one that is dominated by dipole-dipole forces.[20] Despite permanent dipole moments of 1.1 (Ref. 28) and 0.16 D,[29] respectively, for NO $A\ ^2\Sigma^+$ and NO $X\ ^2\Pi$ molecules, dispersion forces dominate when one considers thermal averaging over the molecular orientations.[20,21]

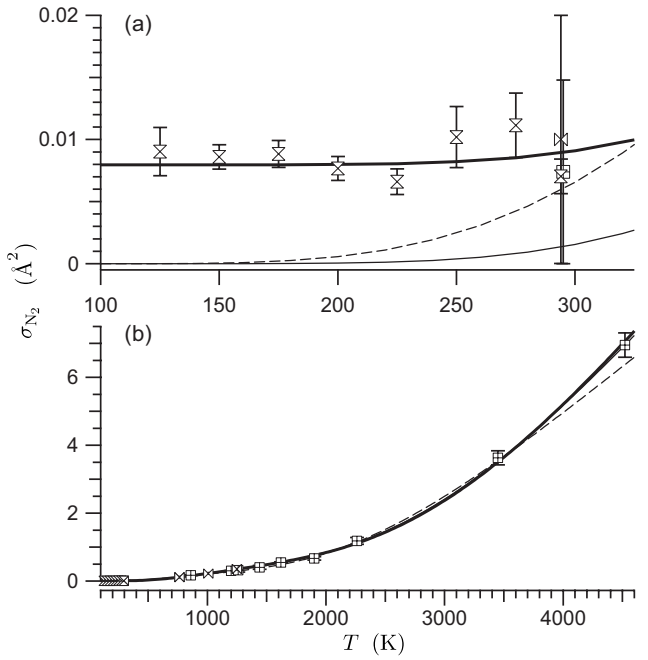

FIG. 6. Temperature dependence of the quenching cross section for N_2. (a) Comparison of current low-temperature measurements and models. (b) Measurements used in global fit for $125\leq T\leq 4500$ K.

C. Quenching by N_2

Figure 6(a) summarizes the current measurements for quenching by N_2. Our room-temperature measurement of σ_{N_2} agrees well with previous measurements,[16,18,23,27,30–32] but there are no previously reported measurements below room temperature. Here, we clearly observe that the quenching cross section remains constant to within the experimental uncertainty for $T<300$ K.

In Fig. 6(b), the abscissa is expanded to display previously reported measurements[4,23] that are included in the current analysis for $T\geq 294$ K. The cross section for quenching by N_2 monotonically increases above 300 K. This behavior is captured well by the harpoon quenching calculations of Paul and co-workers,[6,23,33] which included multiple curve crossings from excited vibrational levels to account for the temperature dependence up to 1900 K. To produce agreement over the full range of temperatures for their shock-tube data,[23] Paul *et al.*[6] recommended the empirical fit shown as the thin dashed curves in Fig. 6. In Ref. 4, we refined the fitting function (thin solid curves) to produce a slightly better fit to our data between 294 and 1249 K.

Although the models recommended in Refs. 4 and 6 agree extremely well with measurements between 294 and 4500 K, they asymptotically approach zero as the temperature decreases, in accord with the harpoon model. The current data, however, indicate that although apparently improbable, collisions with N_2 at low temperature do have a finite quenching cross section. Based on this new observation, we now include a constant term, c_0, in the fitting function [Eq. (6)]. The best-fit value for c_0 is small ($0.008\ \text{Å}^2$) but statistically significant and cannot be explained by quenching by impurities in the bottled gases. The new fitting function, plotted as the thick solid curve in Fig. 6, agrees well with the

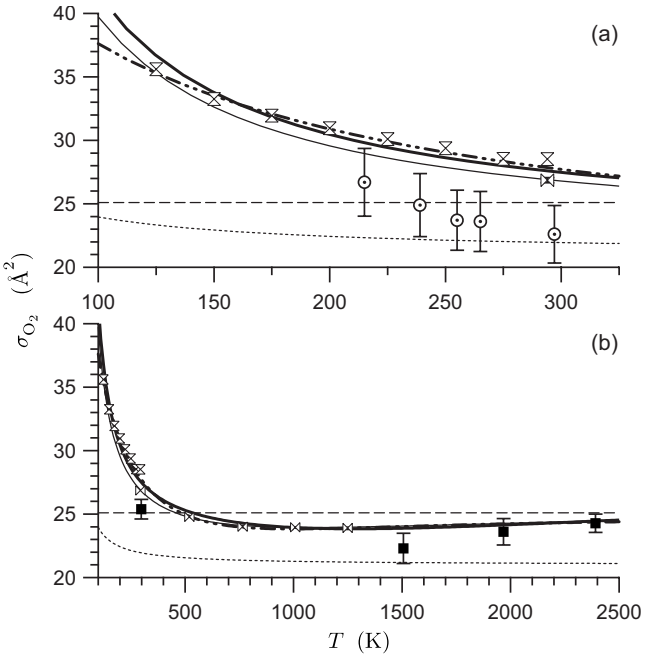

FIG. 7. Temperature dependence of the quenching cross section for O_2. (a) Comparison of current and previous low-temperature measurements and models. (b) Measurements used in global fit for $125 \leq T \leq 2500$ K.

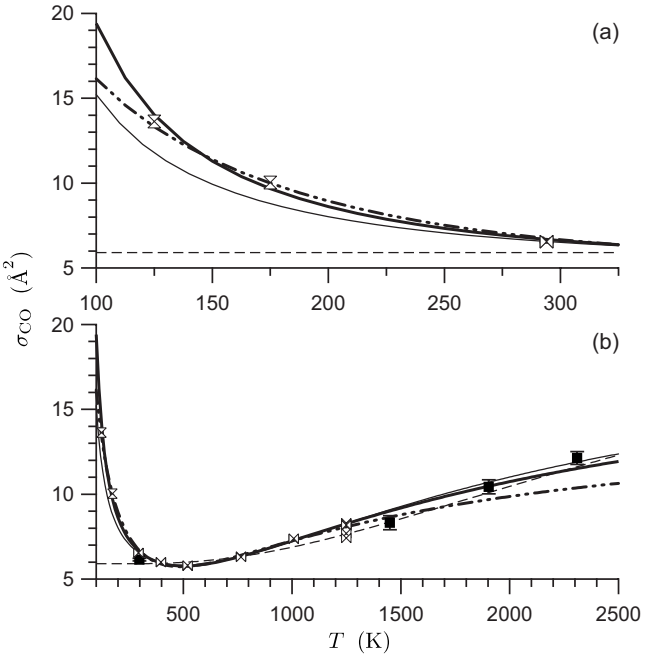

FIG. 8. Temperature dependence of the quenching cross section for CO. (a) Comparison of current measurements and models. (b) Measurements used in global fit for $125 \leq T \leq 2500$ K.

new data for $T<300$ K and differs negligibly from the model recommended in Ref. 4 for $T>300$ K. The best-fit to the data using Eq. (7) is not satisfactory.

D. Quenching by O_2

The current results for quenching by O_2 are shown in Fig. 7. Zhang and Crosley[8] reported the only other low-temperature measurements of cross sections for quenching by O_2, and their results are also shown in Fig. 7(a). The other measurements[4,24] used in the current analysis of the O_2 cross section for higher temperatures are shown in the expanded plot in Fig. 7(b). The earlier temperature-dependent measurements of σ_{O_2} in Refs. 8, 18, and 27 were not included in the analysis because of their lower precision relative to the current measurements and those reported in Ref. 4.

Both sets of low-temperature data display a similar negative temperature dependence that is not predicted by the harpoon model of Paul *et al.*[6] (shown as the thin dashed line in Fig. 7). Zhang and Crosley[8] fitted the temperature dependence using the Parmenter formalism[19] with a potential well depth of 19 cm^{-1}, and the model is shown as the dotted curves in Fig. 7. In Ref. 4, we also unambiguously observed a decrease in the cross section with increasing temperature for $T \geq 294$ K. Based on an empirical fit to the data, we recommended the model shown as the thin solid curve, which is characterized by a significantly larger well depth (41 cm^{-1}) than suggested in Ref. 8. The extrapolation of the model in Ref. 4 to temperatures less than 294 K produces satisfactory agreement with the current measurements [see Fig. 7(a)].

The least-squares fits to the current data and those from Refs. 4 and 24 using Eqs. (6) and (7) are shown as the thick curves in the figure. The best-fit value for c_2 using Eq. (6) corresponds to a well depth of 43 cm^{-1}, which is only slightly larger than the value recommended in Ref. 4. The best-fit value of the power-law exponent in Eq. (7), c_2, is 0.29. According to the multipole expansion of Holtermann *et al.*,[20] this value is consistent with the exponent of 1/3 predicted for dispersion forces, which are expected to be the dominant electrostatic interaction for thermally averaged collisions between NO $A\ ^2\Sigma^+$ and O_2.[21]

Although the weighted least-squares fits using Eq. (6) and (7) are indiscernible for $T>1000$ K and both produce reasonable agreement with the data for the complete temperature range shown in Fig. 7, the least-squares fit using Eq. (7) produces better agreement with the data for $T<1000$ K.

E. Quenching by CO

The current measurements for quenching by CO are shown in Fig. 8. There are no previously reported measurements for temperatures below room temperature. Based on the harpoon model, Paul *et al.*[6] produced excellent agreement with prior measurements for $T \geq 294$ K provided an offset of 6 Å^2 was added to their model to account for the nonzero room-temperature value of the cross section. In Ref. 4, we presented the first clear evidence that the CO quenching cross section increases with decreasing temperature from 520 to 294 K. Based on the measurements in Refs. 4 and 24, we recommended the model shown as the thin solid curve in Fig. 8. The model employed a well depth of 89 cm^{-1} to achieve good agreement with the measurements in Ref. 4.

Extrapolation from 294 to 125 K of the model recommended in Ref. 4 predicts a doubling of the cross section. In view of this rather strong predicted temperature dependence, we made measurements at 175 and 125 K in the current work. As is evident in Fig. 8, the observed temperature dependence is actually slightly stronger than our previous prediction. The best-fit value of c_2 in Eq. (6) obtained in a

least-squares fit to the current data and those from Refs. 4 and 24 correspond to a well depth of 113 cm^{-1}. This value is roughly three times larger than the corresponding well depths for NO $X\ ^2\Pi$ and O_2.

The least-squares fit to these data using Eq. (7) (thick dotted-dashed curve) results in a temperature exponent of 0.86. Although this fit is satisfactory for most of the data, it does not represent the highest-temperature shock-tube data as well as Eq. (6). Unlike the best-fit exponents to the low-temperature dependence of the NO and O_2 cross sections, the value for CO is consistent with low-temperature complex formation via a strong dipole-dipole interaction.[20] The electrostatic interactions between NO $A\ ^2\Sigma^+$ and CO, however, are expected to be similar to those between NO $A\ ^2\Sigma^+$ and NO $X\ ^2\Pi$ because the permanent dipole moments, polarizabilities, and ionization potentials of ground-state CO and NO are comparable. In fact, the dipole-dipole interaction with CO should be weaker than with NO $X\ ^2\Pi$, and the dispersion interaction stronger. Thus the measured temperature dependence is not consistent with the simple picture of quenching facilitated via formation of an electrostatic complex.

VI. CONCLUSIONS

We report measurements of low-temperature cross sections for quenching of NO $A\ ^2\Sigma^+(v'=0)$ by NO, N_2, O_2, and CO using time-resolved LIF excited by a picosecond laser. Low-noise fluorescence signal decays were recorded and fitted with a detailed convolve-and-compare model to accurately measure fluorescence lifetimes. Samples were prepared using high-purity gases and flowed at set pressures through a novel cryogenically cooled fluorescence cell that controlled the gas temperature between 125 and 294 K with a precision typically better than 1 K. The quenching rate coefficients of gas mixtures were determined from the pressure dependence of the fluorescence lifetime, and species-specific quenching cross sections were determined from the dependence of the rate coefficients on the mixture composition.

In addition to providing precise measurements of quenching rate coefficients, the analysis of the pressure dependence of the fluorescence decay rate for over 250 mixtures yielded a natural lifetime of 192 ns for NO $A\ ^2\Sigma^+(v'=0)$. This result corroborates the measurements reported in two of our earlier experiments[4,11] but is approximately 7% shorter than the most recent recommendation of Luque and Crosley.[25,26] Because of the high precision of the current measurements and the reproducibility of this result in three different experimental systems in our laboratory, we recommend use of the value reported here. New measurements of the NO $A\ ^2\Sigma^+(v'=0,1,2)$ lifetimes will be reported in a forthcoming publication.

The current measurements of thermally averaged quenching cross sections improve upon the precision of the only other previously reported low-temperature measurements of quenching by NO and O_2 (Ref. 8) and provide the first low-temperature measurements of quenching by N_2 and CO. The cross sections for quenching by NO, O_2, and CO decrease as temperature increases from 125 to 294 K. This observation is consistent with collision-complex formation at low temperature, in accord with earlier reports of this behavior for NO,[4,8] O_2,[4,8] and CO.[4] Whereas the current measurement of the N_2 cross section agrees with previous room-temperature measurements, the new low-temperature data demonstrate that the cross section has a small constant value of approximately 0.008 $Å^2$ for $T<294$ K and does not decrease to zero as previous models predicted.

We use empirical functions similar to those used previously[4,6,7] to describe the temperature dependence of the cross sections for temperatures ranging from 125 to 4500 K. Weighted fits to the cross sections reported in the present and previous[4,22–24] publications provide a compact parameterization for NO, N_2, O_2, and CO quenching cross sections over this temperature range. The fitting parameters are presented in Table III.

The measured low-temperature dependence of the cross sections for quenching by NO $X\ ^2\Pi$ and O_2 are consistent with a quenching process that is mediated by complex formation dominated by dispersion forces, in accord with the leading term in a multipole expansion of electrostatic forces. On the other hand, this simplified picture does not satisfactorily describe the measured temperature dependence of quenching by CO. Instead quenching by CO is characterized by a significantly stronger temperature dependence that is consistent with complex formation dominated by dipole-dipole forces even though dispersion forces are predicted to be dominant for thermally averaged molecular orientations.[20,21] Although the functional forms of the simplified models used in the current analysis provide excellent representation of the data, a more detailed physical interpretation of the measured quenching dependencies on temperature and species will certainly benefit from more sophisticated theoretical developments including the calculation of the potential energy surfaces for the interaction between NO $A\ ^2\Sigma^+$ and quenching partners.

ACKNOWLEDGMENTS

The authors would like to thank Rachael J. Floyd at Janis Research Co., Inc. for her assistance with the design and customization of the cryostat and Jeffrey A. Gray at Ohio Northern University for many useful discussions. Funding for this research was provided by the U.S. Department of Energy, Office of Basic Energy Sciences, Division of Chemical Sciences, Geosciences, and Biosciences. Sandia is a multiprogram laboratory operated by Sandia Corporation, a Lockheed Martin Co., for the U.S. Department of Energy's National Nuclear Security Administration under Contract No. DE-AC04-94AL85000. C.D.C. was supported by the Air Force Office of Scientific Research, Combustion and Diagnostics Program (Julian Tishkoff, manager).

[1] C. D. Carter and R. S. Barlow, Opt. Lett. **19**, 299 (1994).
[2] N. T. Clemens and P. H. Paul, Phys. Fluids **7**, 1071 (1995).
[3] S. V. Naik, W. D. Kulatilaka, K. K. Venkatesan, and R. P. Lucht, AIAA J. **47**, 839 (2009).
[4] T. B. Settersten, B. D. Patterson, and J. A. Gray, J. Chem. Phys. **124**, 234308 (2006).
[5] J. J. Driscoll, V. Sick, P. E. Schrader, and R. L. Farrow, Proc. Combust.

Inst. **29**, 2719 (2002).
[6] P. H. Paul, J. A. Gray, J. L. Durant, and J. W. Thoman, AIAA J. **32**, 1670 (1994).
[7] M. Tamura, P. A. Berg, J. E. Harrington, J. Luque, J. B. Jeffries, G. P. Smith, and D. R. Crosley, Combust. Flame **114**, 502 (1998).
[8] R. Zhang and D. R. Crosley, J. Chem. Phys. **102**, 7418 (1995).
[9] T. B. Settersten, A. Dreizler, and R. L. Farrow, J. Chem. Phys. **117**, 3173 (2002).
[10] J. W. Daily, W. G. Bessler, C. Schulz, V. Sick, and T. B. Settersten, AIAA J. **43**, 458 (2005).
[11] T. B. Settersten, B. D. Patterson, H. Kronemayer, V. Sick, C. Schulz, and J. W. Daily, Phys. Chem. Chem. Phys. **8**, 5328 (2006).
[12] J. T. Yardley, *Introduction to Molecular Energy Transfer* (Academic, New York, 1980).
[13] H. P. Broida and T. Carrington, J. Chem. Phys. **38**, 136 (1963).
[14] T. Ebata, Y. Anezaki, M. Fujii, N. Mikami, and M. Ito, Chem. Phys. **84**, 151 (1984).
[15] S. Lee, J. Luque, J. Reppel, A. Brown, and D. Crosley, J. Chem. Phys. **121**, 1373 (2004).
[16] I. S. McDermid and J. B. Laudenslager, J. Quant. Spectrosc. Radiat. Transf. **27**, 483 (1982).
[17] H. Zacharias, J. B. Halpern, and K. H. Welge, Chem. Phys. Lett. **43**, 41 (1976).
[18] M. C. Drake and J. W. Ratcliffe, J. Chem. Phys. **98**, 3850 (1993).
[19] H. M. Lin, M. Seaver, K. Y. Tang, A. E. W. Knight, and C. S. Parmenter, J. Chem. Phys. **70**, 5442 (1979).
[20] D. L. Holtermann, E. K. C. Lee, and R. Nanes, J. Chem. Phys. **77**, 5327 (1982).
[21] J. O. Hirschfelder, C. F. Curtiss, and R. B. Bird, *Molecular Theory of Gases and Liquids* (Wiley, New York, 1964).
[22] J. A. Gray, P. H. Paul, and J. L. Durant, Chem. Phys. Lett. **190**, 266 (1992).
[23] J. W. Thoman, J. A. Gray, J. L. Durant, and P. H. Paul, J. Chem. Phys. **97**, 8156 (1992).
[24] P. H. Paul, J. A. Gray, J. L. Durant, and J. W. Thoman, Chem. Phys. Lett. **259**, 508 (1996).
[25] J. Luque and D. R. Crosley, J. Chem. Phys. **111**, 7405 (1999).
[26] J. Luque and D. R. Crosley, J. Chem. Phys. **112**, 9411 (2000).
[27] G. A. Raiche and D. R. Crosley, J. Chem. Phys. **92**, 5211 (1990).
[28] J. A. Gray, R. L. Farrow, J. L. Durant, and L. R. Thorne, J. Chem. Phys. **99**, 4327 (1993).
[29] R. M. Neumann, Astrophys. J. **161**, 779 (1970).
[30] T. Imajo, K. Shibuya, K. Obi, and I. Tanaka, J. Phys. Chem. **90**, 6006 (1986).
[31] G. D. Greenblatt and A. R. Ravishankara, Chem. Phys. Lett. **136**, 501 (1987).
[32] Y. Haas and G. D. Greenblatt, J. Phys. Chem. **90**, 513 (1986).
[33] P. H. Paul, J. A. Gray, J. L. Durant, and J. W. Thoman, Appl. Phys. B **57**, 249 (1993).